Effects of Angle of Attack on Transonic Flutter of a Supercritical Wing

E. Carson Yates Jr.,* Eleanor C. Wynne,† and Moses G. Farmer‡
NASA Langley Research Center, Hampton, Virginia

Flutter calculations have been made by modified strip analysis employing steady-state aerodynamic parameters obtained from published wind tunnel pressure distributions. The results indicate that increasing angle of attack from zero can produce substantial changes in the transonic flutter characteristics that are favorable or unfavorable depending on Mach number and angle of attack. These results correlate well, in a qualitative sense, with the known aerodynamic behavior. The bottom of the transonic flutter-boundary "bucket" is shown to occur at lower Mach number as angle of attack increases. The calculated flutter characteristics are in good agreement with the experimental data at zero angle of attack. At nonzero angles of attack, however, the experiments show sharply declining and backward-turning (multivalued) transonic flutter boundaries that are not indicated by the calculations. Published information indicates that such unconventional flutter boundaries may be caused by viscous effects at low Reynolds number which were not represented in the calculations. The present investigation indicates, however, that the occurrence of these unconventional transonic boundaries appears to be caused, at least to some extent, by variations in static aeroelastic deformation. A mechanism for these phenomena is postulated.

Nomenclature

$a_{c,n}$ = nondimensional distance from midchord to section aerodynamic center measured perpendicular to elastic axis, positive rearward, fraction of semichord
b_r = semichord of wing measured perpendicular to elastic axis at spanwise reference station $\eta = 0.75$ ($b_r = 0.14948$ m)
$C_{l_{\alpha,n}}$ = section lift-curve slope for a section perpendicular to elastic axis
M = freestream Mach number
m_r = mass of wing per unit span at spanwise reference station ($\eta = 0.75$) ($m_r = 2.57$ kg/m)
q = freestream dynamic pressure
V = freestream speed
V_I = flutter-speed index, $(V/b_r\omega_r\sqrt{\mu_r})$
α = angle of attack at wing root
η = nondimensional coordinate measured from wing root along elastic axis, fraction of elastic axis length
μ_r = mass ratio based on spanwise reference station ($\eta = 0.75$), $m_r/\pi\rho b_r^2$
ρ = freestream density
ω = circular frequency of vibration
ω_r = reference frequency, frequency of first uncoupled torsional mode of wing ($\omega_r = 227.23$ rad/s)

Subscripts

1,2 = notation used to distinguish the multiple flutter characteristics in Fig. 5

Introduction

IT is well known that the use of supercritical airfoils, instead of conventional airfoils, can have adverse effects on the transonic flutter characteristics of lifting surfaces. These effects include reduction of transonic flutter speeds[1-3] and increased rate of degradation of flutter speed with small increases in angle of attack (e.g., Ref. 4). Since adequate theories for three-dimensional unsteady transonic flow have not yet been developed and verified, the modified strip analysis first published in 1958[5-11] was used in Ref. 3 to predict (with good accuracy) the subsonic and transonic flutter characteristics for the wing of Ref. 1 at angles of attack near zero. The investigation reported here is an extension of the study of this wing to examine the effects of angle of attack between 0 and 4 deg. Some previously unpublished experimental flutter data for this wing at angles of attack from 0 to 3 deg are also included and compared with calculated results.

The calculated results shown here have been made by the modified strip analysis which has given good flutter results for a broad range of swept and unswept wings at speeds up to hypersonic,[6] including effects of wing thickness[8,9] and angle of attack.[10] In particular, this method was used successfully to calculate transonic flutter characteristics for some swept wings with conventional airfoils,[7] as well as for the present swept supercritical wing.

Flutter Model Parameters

The wind tunnel model used in the present study is that of Ref. 1 and is fully described in that report. Measured geometric, elastic, and inertial properties of this model were used in the flutter calculations. The model geometry is shown in Fig. 1. The frequencies and node lines of the first six measured natural vibration modes and the corresponding modal deflections are given in Figs. 1b and 2 of Ref. 3, respectively. The corresponding generalized masses were determined by the method of displaced frequencies.[12]

These six measured modes were used in all of the flutter calculations. Some collateral calculations made in connection with the study of Ref. 3 indicated that six measured modes were sufficient to converge the flutter results within about 1%.

Flutter Experiments

The flutter tests were conducted in the Langley Transonic Dynamics Tunnel which has a slotted 4.88-m^2 (16-ft^2) test

Presented as Paper 82-0647 at the AIAA/ASME/ASCE/AHS 23rd Structures, Structural Dynamics and Materials Conference, New Orleans, La., May 10-12, 1982; submitted May 28, 1982; revision received April 1, 1983. This paper is declared a work of the U.S. Government and therefore is in the public domain.

*Chief Scientist, Loads and Aeroelasticity Division. Associate Fellow AIAA.
†Mathematician, Loads and Aeroelasticity Division.
‡Aerospace Engineer, Loads and Aeroelasticity Division. Member AIAA.

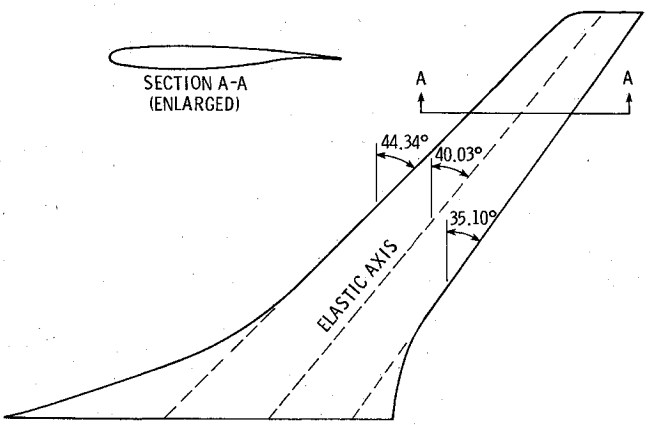

Fig. 1 Supercritical wing flutter model.

section with cropped corners. Air was used as test medium, whereas Freon-12§ was used in the study of Ref. 1. Consequently, the mass ratios μ_r for the present tests are considerably higher than those of Ref. 1 (see also Ref. 3). Flutter data were obtained for wing-root angles of attack of 0, 1, 2, and 3 deg.

Flutter Analysis

Method

The modified strip analysis[5] is formulated for wing strips oriented normal to the elastic axis and is based on stripwise application of Theodorsen-type aerodynamics[13] in which the lift-curve slope of 2π and aerodynamic center at quarter chord are replaced, respectively, by the lift-curve slope and aerodynamic center for the same strip of the three-dimensional wing at the appropriate Mach number M and angle of attack α. The downwash collocation point, where the downwash induced by the aerodynamic load is set equal to the kinematic downwash, is modified accordingly. The circulation function is modified for compressibility by use of two-dimensional unsteady compressible flow theory.[14] Further description and discussion of this method are contained in Refs. 5-7 and 11.

Aerodynamic Parameters

The required spanwise distributions of section lift-curve slope and aerodynamic center were obtained from steady-state surface pressure measurements made by Harris[15] in the Langley 8-ft Transonic Pressure Tunnel. These pressures were integrated numerically as described in Ref. 3 to obtain section-lift and pitching-moment coefficients at 40 stations along the semispan. At each station these section coefficients were numerically spline fitted as a function of angle of attack to obtain a continuous variation with angle of attack. Typical section lift and pitching-moment curves are shown in Figs. 3-5 of Ref. 16.

The spline curves were differentiated analytically to obtain section lift-curve and moment-curve slopes and hence also section aerodynamic center for any desired angle of attack. Typical spanwise distributions of the resulting section lift-curve slope and aerodynamic center, which are input to the flutter calculations, are shown in Fig. 2. (A complete set of $C_{l_{\alpha,n}}$ and $a_{c,n}$ curves for integer values of α, and for both levels of dynamic pressure at each of eight Mach numbers, are shown in Fig. 6 of Ref. 16.) As expected, Fig. 2 and Ref. 16 show that changes in the aerodynamic parameters caused by changes in angle of attack become greater as Mach number increases.

In comparison with the present procedure, the experimental and calculated results of Ref. 3 were all for angle of attack below about 0.3 deg. Consequently, the lift and moment slopes used therein were obtained by fitting straight lines to the section aerodynamic coefficients for the angle of attack nearest zero and the next lowest positive angle of attack.

Since steady-state pressure data are available from Ref. 15 for two levels of dynamic pressure at each Mach number, it is possible to assess the effect on aerodynamic parameters (and hence on flutter) of static aeroelastic deformation of the pressure model, together with an accompanying change in Reynolds number.¶ Consequently, the aerodynamic parameters for both levels of dynamic pressure are used in the flutter calculations.

Mass Ratio

Many of the flutter calculations presented here were made with mass ratio $\mu_r = 27.41$ in order to maintain continuity with the flutter characteristics in Fig. 11 of Ref. 3. Other calculations have been made with higher mass ratios, especially for comparison with the present experimental data.

Results and Discussion

Flutter Calculations for Mass Ratio $\mu_r = 27.41$

Figure 3 shows the effect of angle of attack on the flutter speed index (proportional to the square root of dynamic pressure), calculated by use of the aerodynamic parameters for the lower dynamic pressure at each Mach number (Fig. 2). At each Mach number the effect on the flutter speed index of increasing angle of attack from zero is insignificant for at least the first few tenths of a degree. In the lower subsonic range the effect is minor all the way up to 4 deg. These results are consistent with the concepts of linearized aerodynamic theory. Even at $M = 0.80$ the effect is slight until angle of attack reaches about 3 deg, where a degradation of flutter speed appears to begin. At $M = 0.90$, the degradation begins at about 1 deg. For Mach numbers 0.95 and above, the flutter characteristics are complicated by the appearance of mode changes, closed regions of flutter, and increased sensitivity to variations in angle of attack. At $M = 1.00$, however, the mode changes no longer occur.

The degradation of the flutter speed with increasing angle of attack is generally familiar, but the ensuing rise for Mach numbers 0.95 and above may not be, although it was anticipated from the variation of the aerodynamic parameters (Fig. 2). For $M = 0.80$, the flow over the wing at small angles of attack is subsonic, and the associated variations of $C_{l_{\alpha,n}}$ and $a_{c,n}$ are much like those for $M = 0.25$. As angle of attack approaches 3 deg, however, an embedded supersonic flow region appears forward on the wing upper surface, causing the lifting pressure to increase rapidly there and the aerodynamic centers to move forward more rapidly (Fig. 2b). The effect on flutter speed at 3 deg and beyond is detrimental. For $M = 0.90$, the picture is qualitatively similar, but at this higher Mach number transonic effects start to become significant at about 1 deg angle of attack. Figure 2c shows the related forward movement of aerodynamic center, as well as a rapid increase in $C_{l_{\alpha,n}}$ which occurs at 4 deg. The latter, however, occurs on portions of the span where the forward movement of the aerodynamic centers is relatively not so great. At this higher angle of attack, the supersonic flow region is extensive and is growing primarily aftward (shock moving aft).

At $M = 0.95$, qualitatively similar behavior starts almost at zero angle of attack. The effects of forward-moving aerodynamic center and increasing lift-curve slope over the outer portions of the wing are offset to some extent by op-

§Freon is a registered trademark of E.I. DuPont de Nemours Co., Inc.

¶Reynolds numbers of 2.0 and 3.0×10^6 (based on mean geometric chord) for $M \geq 0.95$ are representative for the 8-ft tunnel tests. However, Ref. 3 indicated the effect of Reynolds number difference at each Mach number to be quite small, at least at the small angle of attack considered in that paper.

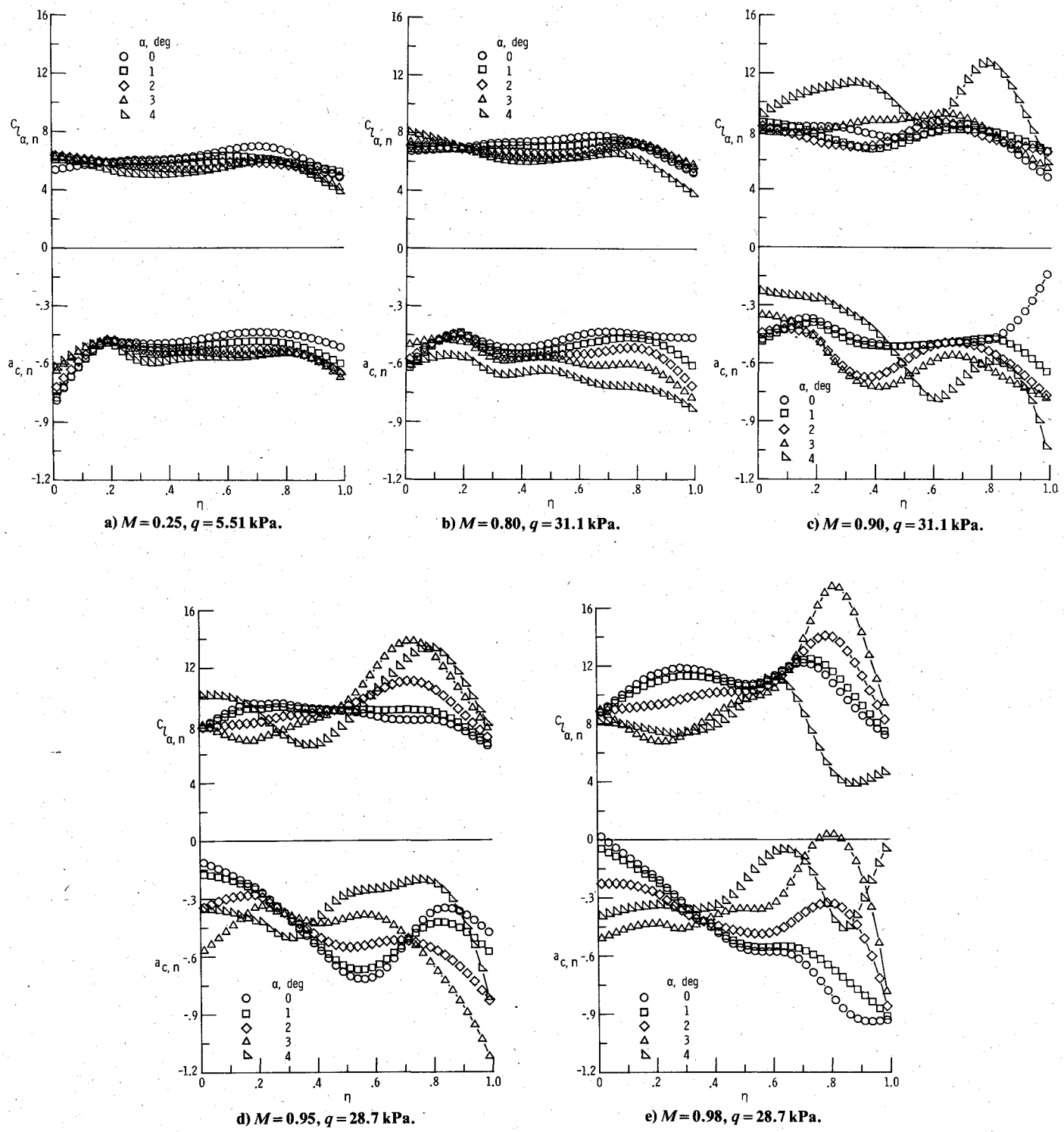

a) $M = 0.25$, $q = 5.51$ kPa. b) $M = 0.80$, $q = 31.1$ kPa. c) $M = 0.90$, $q = 31.1$ kPa.

d) $M = 0.95$, $q = 28.7$ kPa. e) $M = 0.98$, $q = 28.7$ kPa.

Fig. 2 Aerodynamic parameters for flutter analysis.

posite trends over the midsemispan (Fig. 2d). The outer portions dominate, however, because they are weighted more heavily in the flutter motion, and the flutter speed, shown in Fig. 3, declines with increasing angle of attack as at the lower Mach numbers. As angle of attack increases beyond 3 deg, the aftward growth of the supersonic region causes the aerodynamic centers to move aftward again, and the flutter speed increases with increasing angle of attack.

At $M = 0.98$, the supersonic region is extensive even at angles of attack near zero, and its aftward growth with increasing angle causes lift-curve slopes to increase and aerodynamic centers to move aft starting from $\alpha = 0$ deg (Fig. 2e). These are opposing effects on flutter speed. However, the latter dominates and causes flutter speed to rise monotonically as angle of attack increases from zero.

Figure 4 shows crossplots of flutter speed curves such as those in Fig. 3 for integer values of angle of attack. As expected, the Mach number at which the bottom of the "transonic bucket" occurs decreases as angle of attack increases. This result was expected because the onset and development of transonic flow phenomena occur at lower Mach numbers as angle of attack increases. Similar behavior is shown in Ref. 17 for the flutter of two-dimensional airfoils calculated by use of the HYTRAN2 finite difference code. In Fig. 4, the level of flutter speed at the bottom of the bucket varies relatively little with angle of attack except that it is

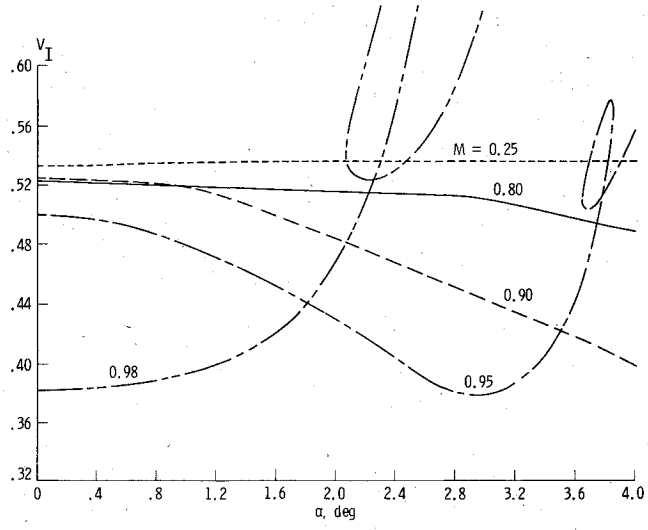

Fig. 3 Effect of angle of attack on flutter at constant Mach number, $\mu_r = 27.41$.

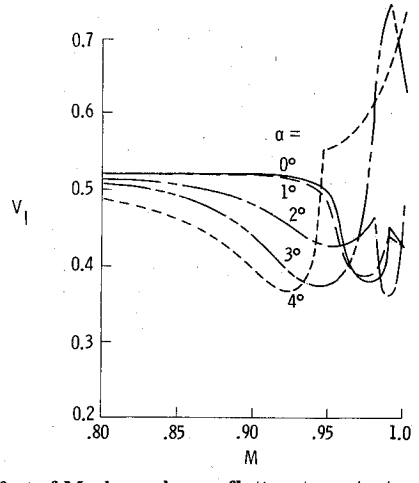

Fig. 4 Effect of Mach number on flutter at constant angle of attack, $\mu_r = 27.41$.

appreciably higher at 2 deg than at higher or lower angles. Moreover, for Mach numbers above 0.98, a second dip occurs which for $\alpha = 2$ deg drops considerably below the primary bucket. Second dips of this sort have been observed in wind tunnel flutter tests[18] and have been speculatively related to disturbances reflected from tunnel walls. In this region of rapid change, aerodynamic data for the present calculations are not available at enough Mach numbers to define the shape of this second dip with precision. Therefore, at any particular angle of attack, the intersection of the primary bucket and the secondary dip is undoubtedly not exactly at the point shown in the figure.

It is possible that shock motion may contribute to the slightly early appearance of the calculated transonic bucket in Ref. 3 and may affect the accuracy of the present result. Use of the aerodynamic parameters obtained from measured steady-state pressure distributions in flutter calculations by the modified strip analysis implies that both shock displacements and viscous effects are incorporated in the same manner as other aerodynamic influences. The steady-state rate of change of shock location with angle of attack, for example, is included in the values of $C_{l_{\alpha,n}}$ and $a_{c,n}$ for each wing section (Fig. 3). These effects, however, are not represented on a purely quasisteady basis in the flutter analysis but are subjected to the same attenuations and phase shifts as all other aerodynamic influences, including the presence of the wind tunnel walls. However, it is well known (e.g., Ref. 19) that the variation with frequency of shock motion and associated phase lag may differ appreciably from the corresponding attenuations and lags for unsteady shock-free flow. The influence of these differences in the present calculations has not been assessed.

Figure 5 shows the effect of static aeroelastic deformation on the calculated flutter characteristics. Aerodynamic parameters for both levels of dynamic pressure have been used at each Mach number as indicated by the solid and dashed curves. The differences between these curves indicate essentially the effect of different static aeroelastic deformations on the aerodynamic model at the two levels of dynamic pressure.** Comparison of the solid and dashed curves in each part of Fig. 5 confirms a result of Ref. 3 that using aerodynamic parameters for the two levels of dynamic pressure caused only minor differences in the calculated flutter speed for angles of attack near zero. Moreover, the differences remain small up to 4-deg angle of attack for Mach numbers up to 0.80 and up to 3 deg for $M = 0.90$ as shown in Fig. 7 of Ref. 16. Thus, as expected, aerodynamic changes caused by static aeroelastic deformation of the aerodynamic model have little effect on flutter speeds in the subsonic range, even up to a few degrees angle of attack. This result is consistent with linearized aerodynamic theory.

As mentioned previously, for Mach numbers 0.95 and above the flutter characteristics are complicated by the appearance of mode changes, accompanied by abrupt changes in flutter frequency (arrows in Fig. 5), closed regions of flutter, and increased sensitivity to both variations in angle of attack and dynamic pressure level.†† However, at $M = 1.00$ the mode changes no longer occur. For these higher Mach numbers, the curves for the different flutter modes have been numbered as an aid in distinguishing them.

Experimental Flutter Data

Experimental flutter data for angles of attack from 0 to 3 deg are presented in Fig. 6, along with calculated flutter characteristics to be discussed subsequently. The solid symbols indicate "hard flutter" (divergent oscillation) points obtained during the tests; the open symbols indicate points of incipient flutter. The circles define the flutter boundary encountered with Mach number and dynamic pressure increasing, whereas the squares indicate flutter points obtained with Mach number and dynamic pressure decreasing. The associated value of mass ratio is indicated beside each hard flutter point. Although relatively few flutter points were obtained, they are sufficient to show the shapes of the flutter boundaries. Figure 6a, for example, shows the occurrence of a conventional transonic bucket for $\alpha = 0$ deg. These data are, in effect, the counterpart in air of the data given in Ref. 1 which were obtained with Freon as the test medium.

On the other hand, for nonzero angles of attack, Figs. 6b-d show flutter boundaries that curve sharply downward and backward toward lower Mach numbers with the sharpest drop (actually, vertical slope) occurring at progressively lower Mach numbers as angle of attack increases. These unconventional transonic buckets are qualitatively similar to those shown in Ref. 4 at angles of attack near zero for a supercritical wing with much less sweep than the present wing. The backward turn of the boundaries in Ref. 4 occurred after a very large decline in the boundary which was attributed to viscous effects at low Reynolds number. Specifically, some evidence indicated that boundary-layer transition strips designed for Reynolds numbers around 2×10^6 did not produce full transition at Reynolds numbers below 1×10^6. The result was an apparent increase in lift-curve slope and

**See ¶ footnote in section entitled Flutter Analysis.

††Because of the complexity of the flutter characteristics shown, the flutter boundaries (lowest flutter speeds) that involve mode changes (Fig. 5) are identified by a bold line.

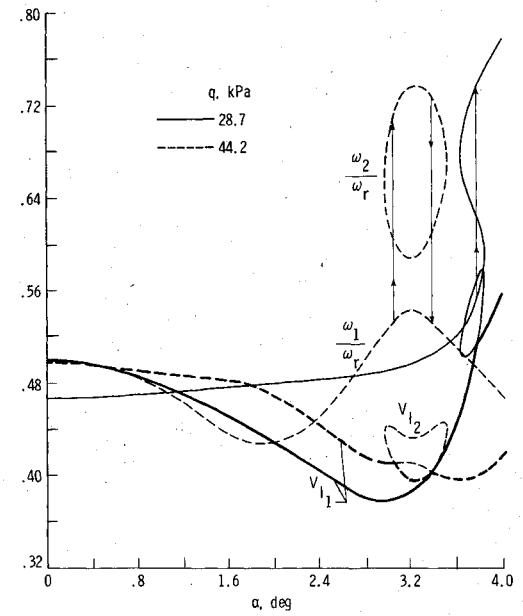

Fig. 5a Effect of aeroelastic deformation on flutter, $\mu_r = 27.41$; $M = 0.95$.

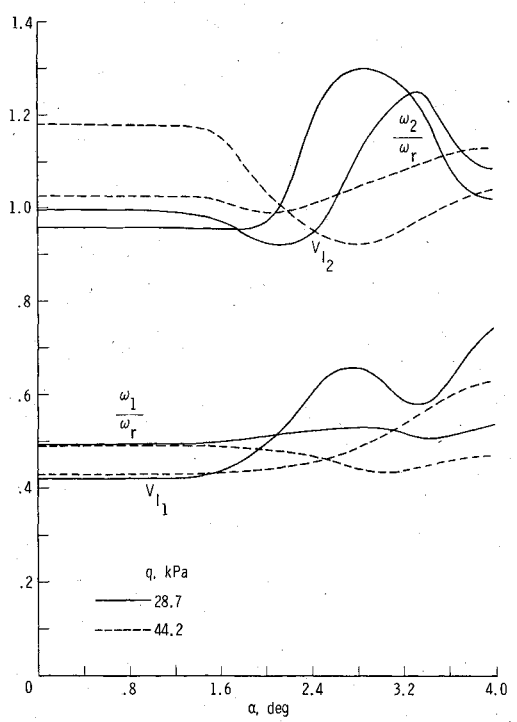

Fig. 5c Effect of aeroelastic deformation on flutter, $\mu_r = 27.41$; $M = 1.00$.

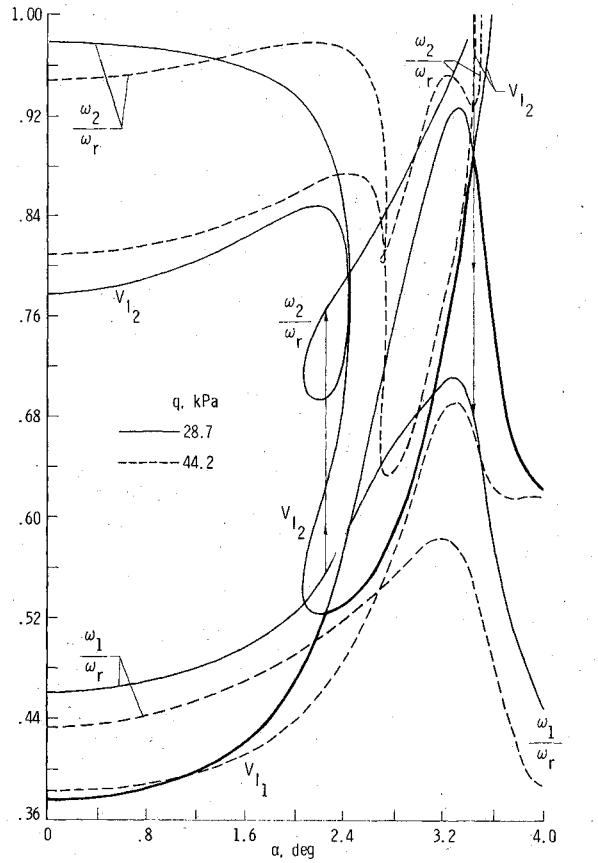

Fig. 5b Effect of aeroelastic deformation on flutter, $\mu_r = 27.41$; $M = 0.98$.

decrease in flutter speed at the lower Reynolds numbers. Similar influences may affect the result shown in Fig. 6. For the present tests in air, the transition-strip grit size and density were selected for a nominal Reynolds number of 1×10^6 based on mean geometric chord. However, at $\alpha = 1$ deg Reynolds number is as low as 0.65×10^6 for the "hard" flutter point at the lowest value of flutter speed index (lowest q), and at $\alpha = 2$ deg, it is as low as 0.42×10^6. The consequences of these low Reynolds numbers have not been examined explicitly in this study. The backward turn in the present boundaries, however, appears to be associated also with variations in the static deformation of the model, as will be discussed below.

The experimental investigation of Ref. 4 did not produce any flutter points on the high Mach number side of the transonic bucket. A few such points were obtained during the present tests (square symbols in Fig. 6), however, and they provide some indication of the width of the unconventional bucket which occurs at nonzero angle of attack.

Comparison of Experiments and Calculations

For comparison with the experimental data, flutter calculations were made using the highest and lowest mass-ratio values for the hard flutter points at each angle of attack. The resulting curves in Fig. 6 show (as in Fig. 5), that using aerodynamic parameters obtained at two levels of dynamic pressure caused only minor differences in flutter speed for all Mach numbers at $\alpha = 0$ deg (Fig. 6a) and for all angles of attack at Mach numbers 0.90 and below.

In Fig. 8 of Ref. 3, the calculated flutter boundary for angle of attack near zero was about 3% conservative (below experiment) in the subsonic range. At much higher mass ratios, in Fig. 6a, the calculated boundary is about 6% conservative relative to the one experimental flutter point near $M = 0.85$. The corresponding flutter frequency is predicted accurately. In Fig. 8 of Ref. 3, the depth of the transonic bucket was calculated accurately, but the onset of the calculated dip was at about 0.04 Mach number lower than the experimentally indicated onset. In Fig. 6a, the onset appears to be calculated accurately, but the calculated bucket is a bit deeper than that obtained from the tests. As in Fig. 9 of Ref. 3, the calculated flutter frequencies in the transonic range are a bit high. Comments in Ref. 3 concerning possible tunnel wall effects and the ratio of model size to tunnel size for the aerodynamic tests (8-ft transonic pressure tunnel) and the flutter tests (transonic dynamics tunnel) are relevant here also.

For $\alpha = 1$ deg (Fig. 6b), the bottom of the unconventional experimental transonic bucket must be slightly above the incipient flutter point at about $M = 0.985$ (open symbol). Even though the calculations did not produce the unconventionally

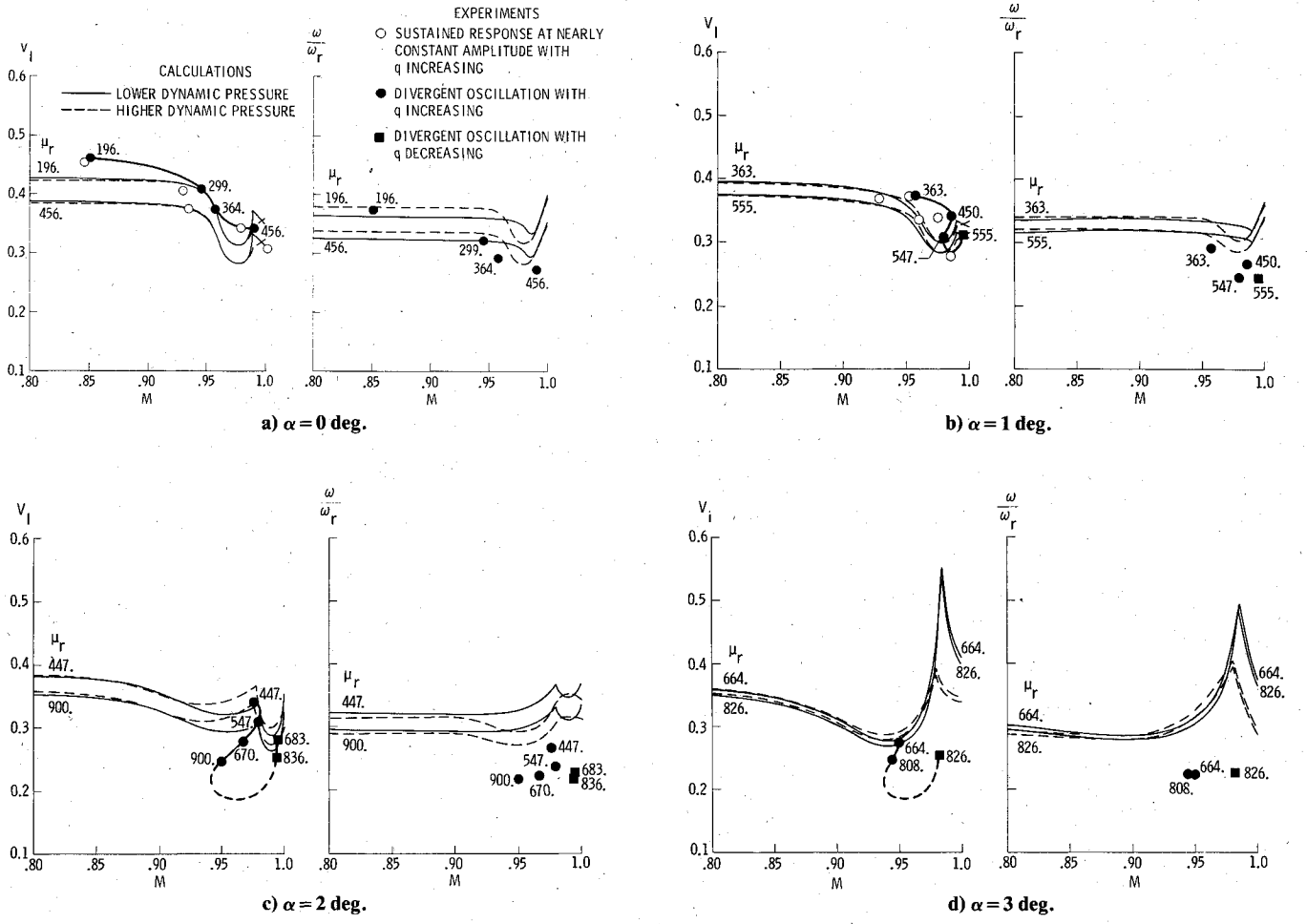

Fig. 6 Comparison of calculated and measured flutter characteristics.

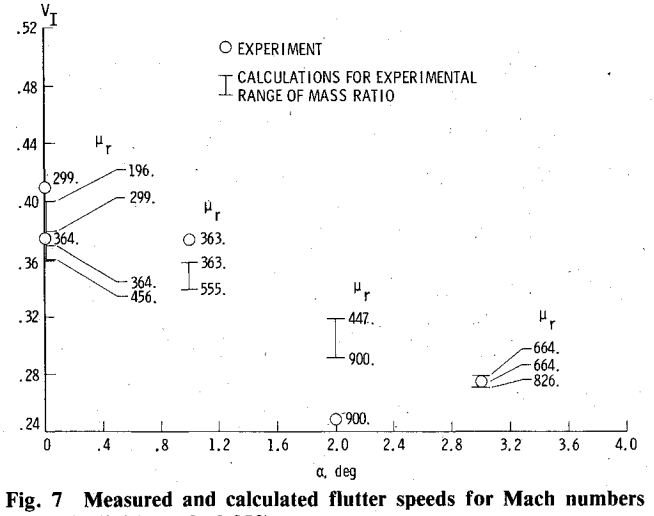

Fig. 7 Measured and calculated flutter speeds for Mach numbers near 0.95 (0.946 < M < 0.958).

shaped bucket, the Mach number and flutter speed level at the bottom of the bucket are predicted satisfactorily by the curve for $\mu_r = 555$.

For $\alpha = 2$ deg (Fig. 6c), the calculated secondary transonic dip provides a reasonable approximation of the upper portion of the unconventional experimental bucket, especially the dashed curve for the higher dynamic pressure level. This observation is probably not significant, however, since there is no such correlation at $\alpha = 3$ deg, and the calculated flutter frequencies are high for both angles.

Finally, Fig. 7 presents an expanded-scale crossplot of data from Fig. 6 as a function of angle of attack. Mach numbers near 0.95 were chosen because that is the only range for which aerodynamic parameters were available for flutter calculations and experimental flutter points were available at all four angles. Agreement between calculations and experiments is good, except at $\alpha = 2$ deg where the calculated value is somewhat high.

Mechanism for the Unconventional Transonic Bucket

The multiple-flutter modes and closed-flutter regions in Fig. 5 have been examined for possible relation to the sharply declining and backward-turning transonic flutter boundaries observed in Fig. 6. Obviously no backward-turning boundaries are predicted here. However, if variations in mass ratio, dynamic pressure level (static aeroelastic deformation), or small changes in Mach number should cause one of the closed flutter regions in Fig. 5 to fall below the primary flutter boundary or cause the sharply declining and backward-turning V_{I_2} mode in Fig. 5b to fall below or to the right of the primary boundary, then a range of angle of attack and Mach number would exist in which a start, stop, and restart of flutter would occur. This would be consistent with a backward-turning boundary as a function of Mach number. In search of these characteristics, extensive calculations have been made for other mass ratios (both higher and lower than 27.41) without indication of the behavior described. Unfortunately, aerodynamic data for the present wing are not available at other Mach numbers between 0.95 and 1.00.

If the unconventional shapes of the experimentally determined flutter boundaries in Fig. 6 are indeed caused largely by low Reynolds number viscous effects, as previously discussed here and in Ref. 4, then it is not surprising that such shapes are not indicated by the present flutter calculations because the aerodynamic parameters used in these

calculations were obtained from pressure distributions measured at Reynolds numbers of 2.0 and 3.0×10^6 for $M\geq0.95$.

The relations between the transonic flutter boundaries calculated with aerodynamic parameters for the two levels of dynamic pressure (Fig. 5) do, however, offer another explanation for the occurrence of the experimentally observed steeply declining and backward-turning flutter boundaries for nonzero angles of attack (Figs. 6b-d). Specifically, the aerodynamic effects of static aeroelastic deformation appear to contribute to this behavior. As mentioned previously, the differences in the aerodynamic parameters for the two levels of dynamic pressure at each Mach number (Fig. 6 of Ref. 16) and the consequent differences in the calculated flutter characteristics (solid and dashed curves in Fig. 5) are attributed primarily to differences in static aeroelastic deformations of the aerodynamic model[15] at the two dynamic pressures. Relative to its size, however, the aerodynamic model was two orders of magnitude stiffer in both bending and torsion than the present flutter model. Consequently, the effects of aeroelastic deformation on the aerodynamic parameters and hence on the calculated flutter speeds are substantially lower than they would be for a more flexible model, such as the flutter model. Even so, for the higher Mach numbers and angles of attack the flutter speed curves calculated with aerodynamic parameters for the two dynamic pressure levels (solid and dashed curves in Fig. 5) differ substantially.

Consider, for example, the relation between the solid and dashed flutter speed curves in Fig. 5a for $M=0.95$ and $\alpha=2$-3 deg, conditions for which Figs. 6c and 6d show the backward turn of the flutter boundary to be well developed. For these conditions, the lower flutter speed in Fig. 5a was calculated with steady-state aerodynamic parameters obtained at the lower dynamic pressure (Fig. 2d). Specifically, the use of aerodynamic parameters for 35% lower dynamic pressure reduced the flutter speed by about 8.5% and the flutter dynamic pressure by about 16.3%. If the aerodynamic model had been more flexible, the indicated fractional change in its test dynamic pressure (35%) would be expected to cause greater changes in static aeroelastic deformation with greater accompanying changes in the aerodynamic parameters and hence greater differences between the two flutter speed curves in Fig. 5a. If the reduction in flutter dynamic pressure were to become as large as the reduction in the "aerodynamic" dynamic pressure, a condition of consistency would exist, and both dynamic pressure levels would represent valid flutter points at the same Mach number and angle of attack. In other words, a multivalued flutter boundary would be indicated. Thus, it is possible that the multivalued backward-turning experimental flutter boundaries in Fig. 6 are caused at least to some extent by changes in static aeroelastic deformation as dynamic pressure and Mach number vary. For comparison, Ref. 17 shows that backward-turning transonic flutter boundaries can be calculated by use of the HYTRAN2 two-dimensional finite difference code for the MBB A-3 supercritical airfoil if variations of the static pitch angle with Mach number and dynamic pressure are permitted. However, no experimental confirmation is provided.

Concluding Remarks

A theoretical and experimental study has been conducted to examine the effects of angle of attack on the transonic flutter characteristics of a highly swept supercritical wing. The steady-state aerodynamic parameters required as input to the modified strip analysis flutter calculations were obtained from published wind tunnel pressure distributions. The results indicate that increasing angle of attack from zero can produce substantial changes in the transonic flutter characteristics that are favorable or unfavorable depending on Mach number and angle of attack. The bottom of the transonic flutter-boundary "bucket" is shown to occur at lower Mach number as angle of attack increases. These flutter results correlate well, in a qualitative sense, with the well-known effects of Mach number and angle of attack on aerodynamic behavior, especially on the development of transonic flow phenomena.

The calculated flutter characteristics are in good agreement with the experimental data at zero angle of attack. At nonzero angles of attack, however, the experiments show sharply declining and backward-turning transonic flutter boundaries that are not indicated by the calculations. Published information indicates that such unconventional flutter boundaries may be caused by viscous effects at low Reynolds number which were not represented in the present calculations because the aerodynamic data available for use in the calculations were for much higher Reynolds numbers than the flutter data. The present investigation indicates, however, that the occurrence of the unconventional transonic boundaries may be caused, at least to some extent, by variations in static aeroelastic deformation.

References

[1] Farmer, M.G., Hanson, P.W., and Wynne, E.C., "Comparison of Supercritical and Conventional Wing Flutter Characteristics," NASA TM-72837, 1976.

[2] McGrew, J.A., Giesing, J.P, Pearson, R.M., Zuhurudding, K., Schmidt, M.E., and Kalman, T.P., "Supercritical Wing Flutter," AFFDL-TR-78-37, 1978.

[3] Yates, E.C. Jr., Wynne, E.C., Farmer, M.G., and Desmarais, R.N., "Prediction of Transonic Flutter for a Supercritical Wing by Modified Strip Analysis and Comparison with Experiment," AIAA Paper 81-0609, 1981.

[4] Houwink, R., Kraan, A.N., and Zwaan, R.J., "A Wind-Tunnel Study of the Flutter Characteristics of a Supercritical Wing," AIAA Paper 81-0651, 1981.

[5] Yates, E.C. Jr., "Calculation of Flutter Characteristics for Finite-Span Swept or Unswept Wings at Subsonic and Supersonic Speeds by a Modified Strip Analysis," NACA RM L57L10, 1958.

[6] Yates, E.C. Jr., "Modified-Strip-Analysis Method for Predicting Wing Flutter at Subsonic to Hypersonic Speeds," *Journal of Aircraft*, Vol. 3, Jan.-Feb. 1966, pp. 25-29.

[7] Yates, E.C. Jr., "Use of Experimental Steady-Flow Aerodynamic Parameters in the Calculation of Flutter Characteristics for Finite-Span Swept or Unswept Wings at Subsonic, Transonic, and Supersonic Speeds," NASA TM X-183, 1959.

[8] Yates, E.C. Jr. and Bennett, R.M., "Use of Aerodynamic Parameters from Nonlinear Theory in Modified-Strip-Analysis Flutter Calculations for Finite-Span Wings at Supersonic Speeds," NASA TN D-1824, 1963.

[9] Yates, E.C. Jr., "Subsonic and Supersonic Flutter Analysis of a Highly Tapered Swept-Wing Planform, Including Effects of Density Variation and Finite Wing Thickness, and Comparison with Experiments," NASA TN D-4230, 1967.

[10] Yates, E.C. Jr. and Bennett, R.M., "Analysis of Supersonic-Hypersonic Flutter of Lifting Surfaces at Angle of Attack," *Journal of Aircraft*, Vol. 9, July 1972, pp. 481-489.

[11] Yates, E.C. Jr., "Flutter and Unsteady-Lift Theory," *Performance and Dynamics of Aerospace Vehicles*, NASA SP-258, 1971, pp. 289-374.

[12] De Vries, G., "Sondage des Systems Vibrants par Massess Additionnelles," *La Recherches Aeronautique*, No. 30, Nov.-Dec. 1952, pp. 47-49.

[13] Theodorsen, T., "General Theory of Aerodynamic Instability and the Mechanism of Flutter," NACA 496, 1935.

[14] Jordan, P.F., "Aerodynamic Flutter Coefficients for Subsonic, Sonic and Supersonic Flow (Linear Two-Dimensional Theory)," British Aeronautical Research Council, R&M 2932, 1957.

[15] Harris, C.D., "Wind-Tunnel Investigation of the Aerodynamic Load Distribution of a Supercritical Wing Research Airplane Configuration," NASA TM X-2469, 1972.

[16] Yates, E.C. Jr., Wynne, E.C., and Farmer, M.G., "Measured and Calculated Effects of Angle of Attack on the Transonic Flutter of a Supercritical Wing," NASA TM 83276, 1982.

[17] Edwards, J.W., Bennett, R.M., Whitlow, W. Jr., and Seidel, D.A., "Time-Marching Transonic Flutter Solutions Including Angle-of-Attack Effects," AIAA Paper 82-0685, 1982.

[18] Sandford, M.C., Ruhlin, C.L., and Abel, I., "Flutter Studies of Simplified Component Models of a Variable-Sweep-Wing Airplane at Mach Numbers Up to 3.0," NASA TN D-3501, 1966.

[19] Ashley, H., "Role of Shocks in the 'Sub-Transonic' Flutter Phenomenon," *Journal of Aircraft*, Vol. 17, March 1980, pp. 187-197.